Manuscript submitted to
AIMS' Journals
Volume **X**, Number **0X**, XX **200X**

doi:10.3934/xx.xx.xx.xx

pp. **X–XX**

NUMERICAL EVALUATION OF ARTIFICIAL BOUNDARY CONDITION FOR WALL-BOUNDED STABLY STRATIFIED FLOWS

Tomáš Bodnár

Department of Technical Mathematics, Faculty of Mechanical Engineering
Czech Technical University in Prague
Karlovo Náměstí 13, 121 35 Prague 2, Czech Republic
and
Institute of Mathematics, Czech Academy of Sciences
Žitná 25, 115 67 Prague 1, Czech Republic

Philippe Fraunié

Mediterranean Institute of Oceanography - MIO
UM 110 USTV - AMU - CNRS/INSU 7294 - IRD 235
Université de Toulon, BP 20132 F-83957 La Garde cedex, France

Petr Knobloch*

Department of Numerical Mathematics, Faculty of Mathematics and Physics
Charles University
Sokolovská 83, 186 75 Prague 8, Czech Republic

Hynek Řezníček

Department of Technical Mathematics, Faculty of Mechanical Engineering
Czech Technical University in Prague
Karlovo Náměstí 13, 121 35 Prague 2, Czech Republic
and
Institute of Mathematics, Czech Academy of Sciences
Žitná 25, 115 67 Prague 1, Czech Republic

(Communicated by the associate editor name)

Abstract. The paper presents a numerical study of the efficiency of the newly proposed far-field boundary simulations of wall-bounded, stably stratified flows. The comparison of numerical solutions obtained on large and truncated computational domain demonstrates how the solution is affected by the adopted far-field conditions. The mathematical model is based on Boussinesq approximation for stably stratified viscous variable density incompressible fluid. The three-dimensional numerical simulations of the steady flow over an isolated hill were performed using a high-resolution compact finite difference code, with artificial compressibility method used for pressure computation. The mutual comparison of the full domain reference solution and the truncated domain solution is provided and the influence of the newly proposed far-field boundary condition is discussed.

2010 *Mathematics Subject Classification.* Primary: 76D50, 76B60, 76D25, 76D10; Secondary: 76D05, 65M06, 65M20.

Key words and phrases. Stratified fluid, finite difference method, Lee waves, flow over a hill, artificial boundary conditions.

* Corresponding author: Petr Knobloch.

1. **Introduction.** The wall-bounded flows appear in many physical applications and are subject of long-lasting theoretical and numerical investigation. The problem of numerical simulation of such flows is necessarily associated with the choice of a bounded computational domain. At the newly created artificial boundaries (i.e. all boundaries except the wall), located at a finite distance from the region of interest, some boundary conditions need to be prescribed. This is necessary from theoretical point of view, to have a well-posed problem, but also from the numerical point of view, to fully determine the numerical solution at the discrete level. The boundary conditions adopted on the artificial boundaries of the computational domain need to be strong enough to guarantee the solvability of the problem, while on the other hand they should be "soft enough" to respect the natural physical behavior of the computed solution fields, rather then forcing them into some pre-defined state.

The problem solved in this paper is motivated by the atmospheric boundary layer flow over an isolated smooth hill, under the conditions of stable stratification. The computational domain was chosen as a three-dimensional rectangular box (cuboid), with six boundaries. One of them, the lower one, is the solid impermeable wall, in our case representing the terrain surface, with the low, smooth isolated hill. This is the only physical boundary of the computational domain. All the other boundaries are artificial. When the coordinate system (attached to the computational domain) is aligned with the mean flow, one of the artificial parts of the boundary can be considered as inlet and one (the opposite one) as outlet. The lateral and upper boundaries are kind of far-field open boundaries. The focus of this paper is on these far-field artificial boundaries and the associated boundary conditions.

In the setup described above, the far-field boundaries (both the upper and lateral) have some common characteristics. The flow is supposed to be almost (but not necessarily exactly) parallel to the boundary, with the tangential velocity component being in general dominant over the normal one. The (boundary-) normal velocity component cannot be neglected (considered to vanish) without significantly affecting the flow in the computational domain. The flow in such far-field regions can be considered as convection-dominated, except a narrow near wall part of the lateral boundaries.

The mathematical modeling and numerical simulation of wall-bounded, convection-dominated flows in this setup is in general very sensitive to the artificial boundary conditions applied at far-field boundaries. In the homogeneous non-stratified fluid flow case, the flow perturbations caused by the wall-mounted obstacle (hill in our case) are well localized, affecting a region in space being dependent on the size of the obstacle. The outer boundaries of the computational domain can usually be shifted "far enough" from the perturbed region of interest. Also the computational grid being coarsened towards those far-field boundaries is easy to construct. Thus it is natural and relatively easy to adopt and prescribe the far-field boundary conditions based on the undisturbed "outer flow" limit, e.g., assuming vanishing some flow components or their gradients, imitating some background fully developed flow.

The stratified case is in this respect much more problematic. Every obstacle over which the stratified fluid flows, induces flow perturbation that generates large gravity waves field that perturbs the flow. It has a wavelength dictated by the strength of the stratification (background density gradient) rather than being related to the size of the obstacle. Also the spatial extent of the gravity waves is much larger than the characteristic size of the obstacle (see e.g. [1], [2]). Thus in general the far-field boundary of the computational domain cannot be placed "far enough" to consider

the flow to be unperturbed. Also due to the presence of the gravity waves in the far field, the computational grid cannot be excessively coarsened without significantly affecting the solution.

The aim of this paper is to propose and test a boundary conditions setup allowing to numerically resolve the flow, including possible gravity waves, in the whole computational domain, up to the far-field boundaries. The efficiency of the proposed far-field boundary setup is tested by comparing the numerical solution obtained for large and truncated computational domain. The goal is to show that the proposed computational setup provides a numerical solution on the truncated domain that differs only marginally from the reference solution obtained on much larger domain.

2. Mathematical model.

2.1. **Governing equations.** The full incompressible, viscous (laminar), variable density model can be written as:

$$\begin{aligned} \mathrm{div}\boldsymbol{u} &= 0 \quad , & (1)\\ \frac{\partial \rho}{\partial t} + \boldsymbol{u}\cdot\mathrm{grad}\,\rho &= 0 \quad , & (2)\\ \rho\left(\frac{\partial \boldsymbol{u}}{\partial t} + \mathrm{div}(\boldsymbol{u}\otimes\boldsymbol{u})\right) &= -\mathrm{grad}\,p + \mathrm{div}2\mu\mathbb{D} + \rho\boldsymbol{g} \quad , & (3) \end{aligned}$$

where μ is the dynamic viscosity, tensor $\mathbb{D} = \frac{1}{2}(\mathrm{grad}\,\boldsymbol{u} + \mathrm{grad}\,\boldsymbol{u}^T)$ is the symmetric part of velocity gradient, and $\boldsymbol{g}$ is the gravitational acceleration. These equations lead to the set of governing equations for the velocity $\boldsymbol{u}(\boldsymbol{x},t)$, density $\rho(\boldsymbol{x},t)$ and pressure field $p(\boldsymbol{x},t)$. This model is sometimes called the *non-homogeneous Navier-Stokes equations*.

This system is used as a starting point to develop the so-called Boussinesq approximation. The pressure and density fields are assumed to be perturbations of the hydrostatic equilibrium state:

$$\begin{aligned} \rho(\boldsymbol{x},t) &= \rho_0(\boldsymbol{x}) + \rho'(\boldsymbol{x},t) \qquad i.e. \qquad \rho(x,y,z,t) = \rho_0(z) + \rho'(x,y,z,t) \quad ,\\ p(\boldsymbol{x},t) &= p_0(\boldsymbol{x}) + p'(\boldsymbol{x},t) \qquad i.e. \qquad p(x,y,z,t) = p_0(z) + p'(x,y,z,t) \quad , \end{aligned}$$

where the background density and pressure fields are linked by the hydrostatic relation:

$$\mathrm{grad}\,p_0 = \rho_0\boldsymbol{g} \qquad i.e. \qquad \frac{\partial p_0}{\partial z} = \rho_0 g \quad ,$$

with the gravity force (acceleration) expressed as $\boldsymbol{g} = (0,0,g)$. This leads to a rearranged momentum equation:

$$\frac{\partial \boldsymbol{u}}{\partial t} + \mathrm{div}(\boldsymbol{u}\otimes\boldsymbol{u}) = \frac{1}{\rho}\Big(-\mathrm{grad}\,p' + \mathrm{div}2\mu\mathbb{D} + \rho'\boldsymbol{g}\Big) \quad . \qquad (4)$$

So far only decompositions and rearrangements were applied to the governing system, no approximations were made, and thus the momentum equation (4) is equivalent to the original equation (3).

The *Boussinesq approximation* is obtained from the full system of non-homogeneous incompressible Navier-Stokes equations by replacing the complete density ρ in the convective terms by a suitable (fixed in space and time) characteristic density ρ^* and by using the notation p for the pressure perturbation. This immediately leads to the approximate set of governing equations, the so-called Boussinesq

approximation[1]:

$$\begin{aligned} \operatorname{div}\boldsymbol{u} &= 0 \quad , \\ \frac{\partial \rho}{\partial t} + \boldsymbol{u}\cdot\operatorname{grad}\rho &= 0 \quad , \\ \frac{\partial \boldsymbol{u}}{\partial t} + \operatorname{div}(\boldsymbol{u}\otimes\boldsymbol{u}) &= \frac{1}{\rho^*}\Big(-\operatorname{grad} p + \operatorname{div} 2\mu\mathbb{D} + (\rho-\rho_0)\boldsymbol{g}\Big) \quad . \end{aligned}$$

This is the system that was used to compute the fields of velocity $\boldsymbol{u}(\boldsymbol{x},t) = (u(\boldsymbol{x},t), v(\boldsymbol{x},t), w(\boldsymbol{x},t))$, pressure (perturbation) $p(\boldsymbol{x},t)$ and density $\rho(\boldsymbol{x},t)$ in the numerical simulations presented in this paper.

2.2. **Problem of boundary conditions.** The outflow as well as far-field boundary conditions for incompressible flow models have been subject of research for a long time. As noted above, the boundary conditions are needed either to complement the governing equations to form a well-posed mathematical problem, or to fully determine the numerical solution at the discrete level. In any case, when modelling a physically relevant problem, they should also respect the physical nature of the problem.

This paper is motivated by the incompressible non-homogeneous (variable density) stratified flow. The same problem, although being less apparent, is also present in the homogeneous constant density case, represented by the classical incompressible Navier-Stokes equations. Thus most of the below presented discussion and conclusions can easily be translated into the traditional homogeneous Navier-Stokes based models.

Before presenting our tested newly proposed boundary conditions setup, let us shortly mention two approaches that may come to question when dealing with the above describe flows models.

Do-nothing condition is based on the paper by Heywood, Rannacher and Turek [8]. The do-nothing (DN) condition is seen as a natural type of pressure-velocity outflow condition implicitly embedded in the variational formulation of the problem. This condition (for sufficiently smooth solution) implies that on the outlet boundary:

$$p = \mu\frac{\partial u_n}{\partial n} \qquad \text{and} \qquad \mu\frac{\partial u_\tau}{\partial n} = 0 \quad , \tag{5}$$

where u_n and u_τ denote the (boundary-)normal and tangential components of velocity. It means that the homogeneous Neumann condition is applied to tangential components of velocity vector while the normal derivative of normal velocity component is used to set the Dirichlet condition for pressure. This condition was successfully used in many simulations in the past decades. Recently, in the paper by Braack and Mucha [6], the so called directional do-nothing (DDN) condition was introduced and studied. In most cases the do-nothing condition performs very well, however, for our purposes it does not seem to be suitable. We are solving a convection-dominated case where the viscosity is small and so are the normal derivatives of velocity. Thus it gives an almost constant (close to zero) pressure along the boundary. Moreover the assumption of homogeneous Neumann condition for the tangent velocity components is very strong and sometimes non-physical, especially in the stratified case.

[1] See [3] for the formal development of the model.

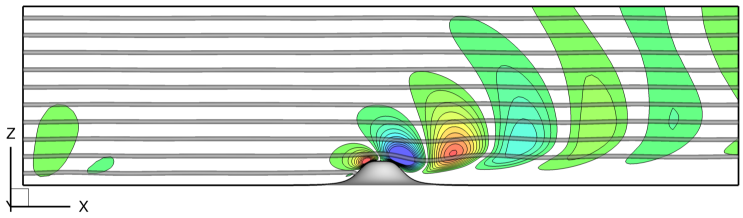

FIGURE 1. Vertical velocity contours and flow streamlines in the plane of symmetry.

Radiation condition was introduced by Orlanski [11] and further extended e.g. by Marchesiello in [10]. It is being used (in many variants) for various wave phenomena simulations, mainly in the environmental fluid mechanics. It is designed as non-reflective (or transparent) boundary condition to allow the traveling waves to leave the computational domain without being reflected back to the computational field. Roughly speaking, it is based on setting non-homogeneous Neumann condition for the considered variable, using the numerical estimate of the traveling wave speed. This condition is however designed for traveling waves and for stationary waves it will degenerate to the simple homogeneous Neumann condition for all flow quantities. Namely in the case considered in this paper it will reduce to

$$\frac{\partial u_n}{\partial n} = 0, \qquad \frac{\partial u_\tau}{\partial n} = 0 \quad \text{and} \quad \frac{\partial p}{\partial n} = 0 \qquad .$$

The homogeneous conditions are often used as far-field conditions, assuming that at the far-field boundary the boundary-normal change of the variable is negligible. This might be acceptable in homogeneous (non-stratified) flows, but it is certainly far from being applicable in stratified cases including gravity waves in the far field.

Preliminary example. When the stratified flow over a hill is solved[2], the solution contains large field of gravity waves on the lee side of the hill. These waves can best be visualized either using the flow streamlines, showing the characteristic wavy pattern, or by contours (or isosurfaces) of the vertical component of velocity. The regions of ascending/descending flow form a typical quasi-periodic pattern behind the hill. Such situation is shown in Fig. 1, where the vertical velocity contours are drawn together with streamlines in the plane of symmetry of the computational domain (and of the flow field). The same case can be visualized in 3D, using the isosurfaces of vertical velocity shown in Fig. 2, where the result is first visualized on larger domain (left) and then a detail of the same result, truncated to the size of a smaller domain, is shown (right). Going back to 2D visualization, the vertical velocity contours in the plane of symmetry are shown in Fig. 3. The position of the horizontal cutting plane, that is reducing the vertical size of the domain, is marked by a dashed line. This result will now be taken as a reference solution. The aim is to use only the small domain, compute the solution just on this truncated domain, applying the artificial boundary conditions on the far-field (upper and lateral) boundaries, and compare this truncated domain solution with the one obtained on the larger domain. The goal is to get numerical solution (on the truncated domain)

[2]The results presented in this section only serve as illustration of the problem of boundary conditions. See Section 3.2 for detailed description.

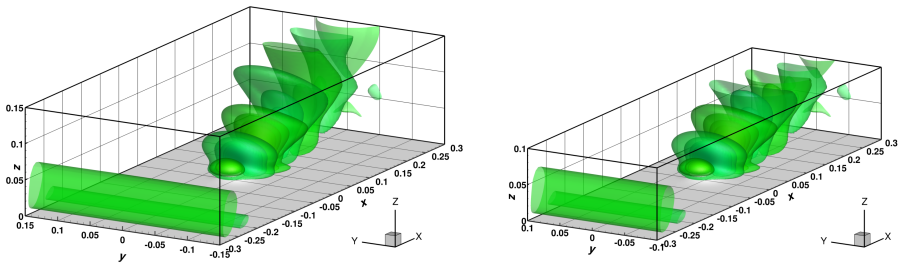

complete solution truncated solution

FIGURE 2. Vertical velocity isosurfaces.

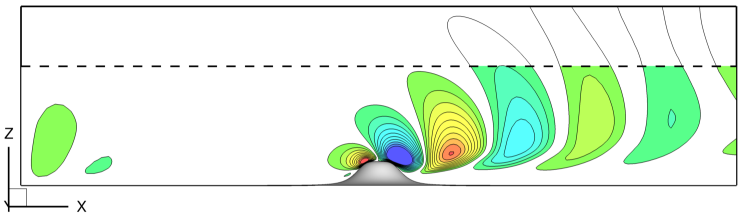

FIGURE 3. Vertical velocity contours in the plane of symmetry – *truncated solution*.

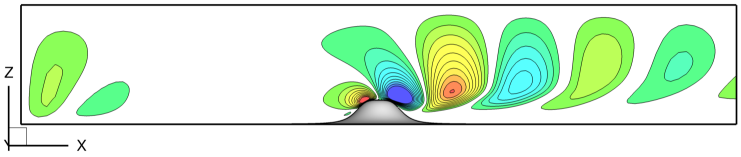

FIGURE 4. Vertical velocity contours in the plane of symmetry – *truncated domain* – $\frac{\partial p}{\partial n} = 0$.

that will be not disturbed and significantly affected by the presence of the artificial far-field boundaries and the associated boundary conditions.

Now, let us consider only the smaller, truncated computational domain (see Section 3.1). For the purpose of this example, let us assume that at the far-field boundaries all flow variables, except pressure, are extrapolated (e.g. linearly[3]). For pressure, the homogeneous Neumann condition is used. Solving now the same case as above, but only on the small domain with the above mentioned artificial boundary conditions, the vertical velocity field shown in Fig. 4 was obtained in the plane of symmetry, instead of the results shown in Fig. 3.

From the direct comparison of the results shown in Figs. 3 and 4 is obvious, that the truncation of the computational domain and mainly the homogeneous Neumannn condition used for pressure, have notable impact on the obtained numerical solution. The basic gravity waves flow pattern remains essentially the same (at least close to the hill), however the vertical velocity contours are severely abrupt

[3]It is possible to show that the linear extrapolation is equivalent to the use of one-sided first order approximation of the derivative in the corresponding direction.

close to the upper boundary. The enforced zero normal pressure derivative seems to block the corresponding boundary-normal flow component. In fact, the same influence of the zero normal pressure derivative (homogeneous Neumann) condition can be observed on the lateral boundaries, where again the boundary normal (transversal) velocity component v is blocked. Figs. 5 and 6 show again, side by side, the truncated solution from larger domain with the results obtained on the smaller (truncated) domain (applying the artificial boundary conditions using homogeneous Neumann condition for pressure).

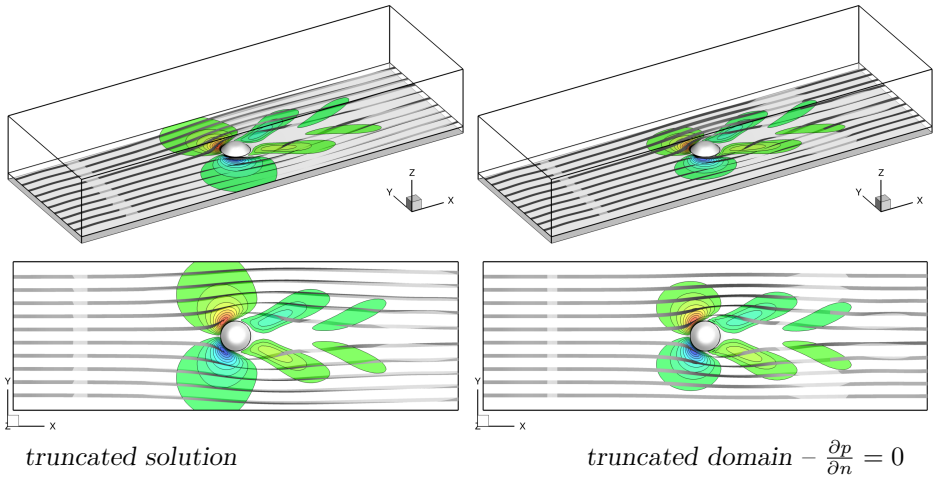

FIGURE 5. Contours of the transversal velocity component v and flow streamlines.

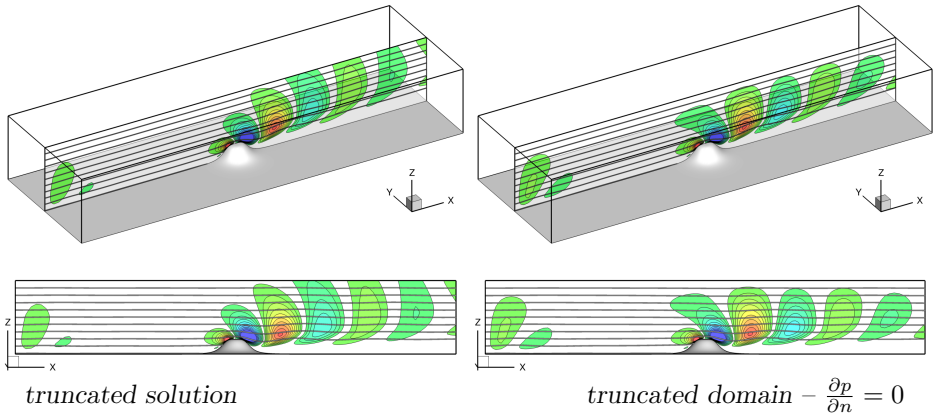

FIGURE 6. Contours of the vertical velocity component w and flow streamlines.

The blocking of boundary normal velocity component is already evident from the slices shown in Figs. 5 and 6, but the most apparent differences can be observed in a direct comparison of the 3D isosurfaces of the transversal and vertical velocity components shown in Figs. 7 and 8.

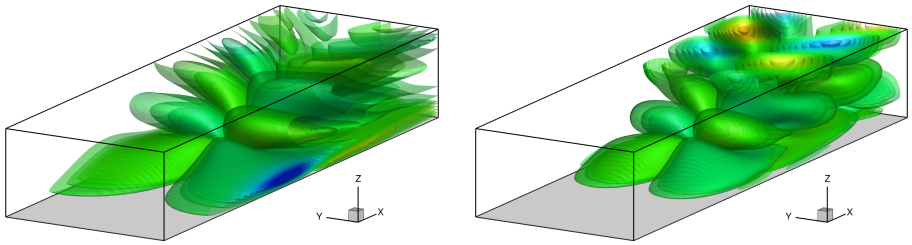

FIGURE 7. Isosurfaces of the transversal velocity component v.

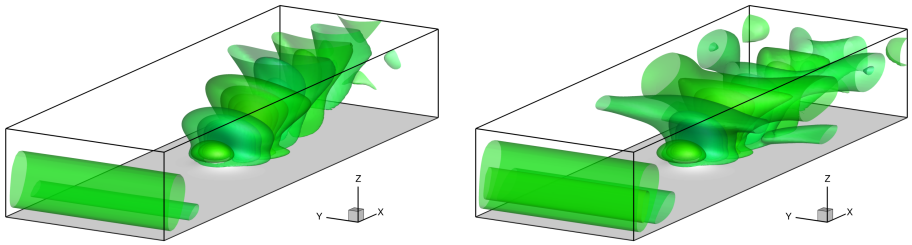

FIGURE 8. Isosurfaces of the vertical velocity component w.

The presented illustrative comparison of the truncated solution from a larger domain with the solution obtained using standard artificial boundary conditions on a smaller (truncated) domain shows significant differences. Although the truncated domain solution can be considered good enough away from the far-field boundaries, close to the hill, it is evident that this solution is incorrect (or at least very inaccurate) close to the artificial far-field boundaries.

Proposed convective pressure derivative boundary condition. Motivated by the above demonstrated failure of the homogeneous Neumann condition for pressure and by the previous tests summarized e.g. in [4, 5] the following non-homogeneous Neumann condition for pressure is proposed:

$$\frac{\partial p}{\partial n} = \rho^* |\boldsymbol{u}| \frac{\partial u_n}{\partial n} \qquad , \tag{6}$$

Here u_n is the wall-normal component of the velocity and $|\boldsymbol{u}|$ is the local velocity magnitude. This condition is applied to pressure at far-field, while the remaining variables are just extrapolated (e.g. linearly) from the interior of the domain to the boundary points.

The essential logic behind the proposed *convective pressure derivative* (CPD) condition is based on the use of the (boundary) normal derivative of the normal velocity component as an indicator of the velocity change "across" the artificial boundary. It is assumed that the local normal velocity change is related to the normal pressure difference. The multiplicative scalar term $\rho^*|\boldsymbol{u}|$ is added as a scaling factor (between the pressure and velocity derivative) to keep the proper dimension of the convective term in the Navier-Stokes equations. For further discussion of the proposed CPD condition (6) see Section 4.

3. **Numerical simulations.** The numerical simulations presented within this paper were designed and performed in order to computationally demonstrate the influence and efficiency of the far-field boundary condition setup associated with the convective pressure derivative condition (6).

The computational test case is motivated by the towing tank laboratory experiments described in [9] and numerical simulations from [7]. This is however just a starting point and the actual configuration of our numerical test cases differs substantially in several aspects from the above mentioned papers.

The numerical solver used to obtain the results presented in this paper is a three-dimensional extension of the method used and described in [1, 2]. It uses a compact finite-difference discretization in space and Strong Stability Preserving (SSP) Runge-Kutta (RK) time integration. Here the sixth-order spatial discretization was combined with third-order SSP RK method in (pseudo-)time. The artificial compressibility was used to compute the pressure and to enforce the divergence-free constraint. In order to smooth the high frequency numerical oscillations, the eight order compact low-pass filter was used. This method built into our in-house developed code was tested (in its 3D version) e.g. in [3], while the essential features are inherited from the 2D version used in [1, 2].

3.1. **Computational setup.** The computational domain is chosen as a bounded part of a half-space, with a rotationally symmetric hill placed on a wall. The 3D computational block has a size $L_x \times L_y \times L_z$, with the z coordinate pointing in vertical direction (against the gravitational acceleration) and the x coordinate pointing in the free stream direction. The hill shape is the same as in [9], resp. [7], i.e. the surface elevation is given by $z_s(r) = h/\left(1 + (r/h)^4\right)$, where r denotes the distance from the hill symmetry axis. The parameter (length scale) h represents the maximum hill height (set to $2cm$ in this case), as well as the hill half width[4].

In order to compare the numerical solution obtained on the truncated domain (using the artificial far-field conditions), with the reference solution from the larger domain, two computational domains were used. The larger domain is extended (with respect to the small one) both vertically (up) and horizontally (on both sides) by a length $H = L_z/2$. So the upper and lateral boundaries are shifted by H and the corresponding computational grid is extended. Both domains are shown in Fig. 9, where the truncated standard domain is emphasized by the red color. The

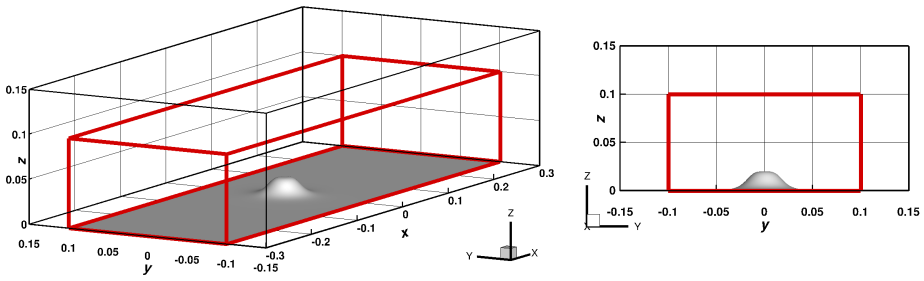

FIGURE 9. Computational domain and its extension.

[4]The width of the hill at the height of $z = h/2$ is $2h$.

standard (smaller, truncated) domain dimensions, in terms of maximum hill height h, are $L_x = 30h$, $L_y = 10h$, $L_z = 5h$. The hill is placed (together with the origin of the coordinate system) at the center of this domain base, i.e., at the position $L_x/2 = 15h$ from the inlet, at the plane of symmetry.

The computational grid is structured, wall fitted, smoothly refined close to the hill. The smaller, truncated domain grid has 156×66×56 cells. For the larger domain, this existing small grid is just extended by adding regularly spaced additional grid points, so the final grid size is 156×86×74 cells. On the overlapping common part of both domains the grid is identical. The minimum cell size is $\Delta x = \Delta y = 0.2cm$ and $\Delta z = 0.1cm$.

Boundary conditions. The standard computational setup used in the below discussed series of simulations is based on the following boundary conditions:

- **Inlet** ... The velocity profile $\boldsymbol{u} = (u(z), 0, 0)$ is prescribed. The horizontal velocity component u is given by the second order polynomial profile $u(z) = U_*\big(2\tilde{z} - \tilde{z}^2\big)$, where non-dimensional height $\tilde{z}$ is defined using the boundary layer thickness as $\tilde{z} = z/(5h/2)$. Above the height $z = 5h/2$, the profile is extended by the constant velocity $U_\infty = U_*$. Density perturbation $\rho' = \rho - \rho_0$ is set to zero, i.e. $\rho = \rho_0(z)$. Homogeneous Neumann condition is used for pressure.
- **Outlet** ... All velocity components and also the density (perturbation) are extrapolated. Pressure is set to a constant (zero).
- **Wall** ... No-slip conditions are used on the wall, i.e. the velocity vector is set to $\boldsymbol{u} = (0, 0, 0)$. The density is extrapolated. Homogeneous Neumann condition is used for pressure.
- **Far field** ... On upper as well as lateral boundaries all velocity components and also the density are extrapolated. The non-homogeneous condition (6) is used for pressure.

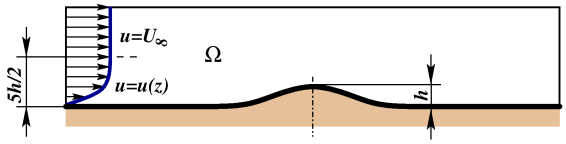

FIGURE 10. Inlet velocity profile setup.

In the simulations shown hereafter, the fluid is characterized by the density $\rho^* = 1000\ kg \cdot m^{-3}$ and dynamical viscosity $\mu = 10^{-3} kg \cdot m^{-1} \cdot s^{-1}$. The linear background density profile is defined by $\rho_0(z) = \rho^* + \gamma \cdot z$, with the (stable) vertical density gradient $\gamma = -25\ kg \cdot m^{-4}$. The gravitational acceleration acts against the z coordinate, so $\boldsymbol{g} = (0, 0, g)$ with $g = -10m \cdot s^{-2}$. The hill height was set to $h = 2cm = 0.02\,m$ and the velocity $U_* = 1\ cm \cdot s^{-1} = 0.01\ m \cdot s^{-1}$.

3.2. **Numerical results.** The results of the above described model are presented here in the form of isosurfaces and contours of selected flow quantities. Unless stated otherwise, the whole computational solution is shown, up to the boundary, without any truncation or cut-off. For the large domain[5], the results are sometimes

[5]The reference solution computed on the larger domain was obtained using the CPD condition in the far-field. See Section 3.3 for further details and discussion concerning this choice.

truncated to the size of the small domain, to allow for a direct comparison as in Section 2.2. This is essential to assess the effects of boundary conditions in the proximity of artificial boundaries of the computational domain.

The transversal velocity contours, plotted at the horizontal slice of the domain placed at $z = h/2$ are shown in Fig. 11. The solution obtained using the homogeneous Neumann pressure conditions shows that the transversal velocity vanishes (is blocked) at the lateral boundaries. This is however in contradiction with the reference truncated solution from the larger domain. The application of the new non-homogeneous CPD condition provides results that are in this respect closer to the reference solution, allowing the transversal flow passage through the lateral boundaries.

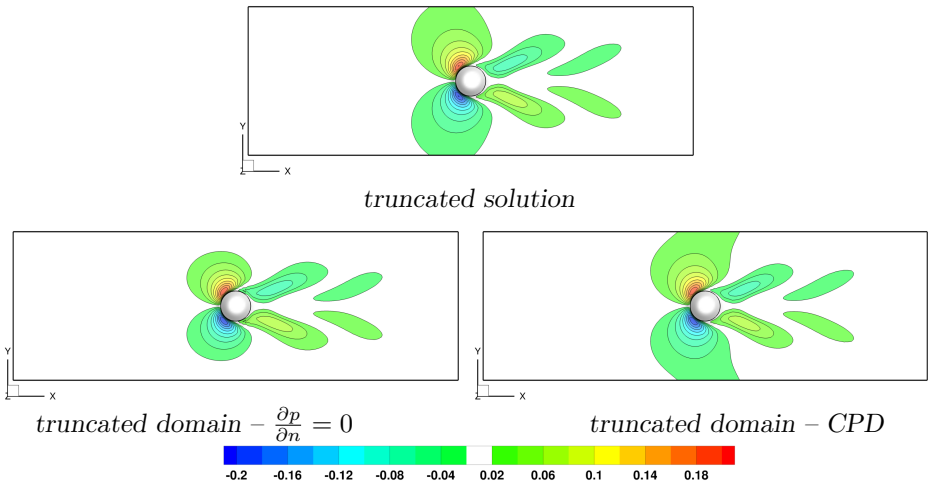

FIGURE 11. Contours of the transversal velocity component v - nondimensionalized $\widetilde{v} = v/U_*$.

The same kind of comparison can be made for the vertical velocity contours plotted in the plane of symmetry in Fig. 12. While the homogeneous Neumann pressure condition blocks the vertical flow through the upper boundary, both the truncated solution from the larger domain and the truncated domain solution using the CPD condition, do not exhibit this singularity. Although the agreement between the truncated solution and the truncated domain solution using CPD condition is not perfect, the improvement over the homogeneous Neumann solution is evident, at least removing the artificial flow blocking at the upper boundary. The improvement of the solution is most apparent where the discrepancy was most visible, i.e., in the very different shape of the isosurfaces of the velocity components, already shown in the demonstration of the failure of the homogeneous Neumann condition shown in Figs. 7 and 8. Adding now the new convective pressure derivative condition to the comparison, the great improvement using this condition can be seen for both the transversal component v in Fig. 13 as well as for the vertical velocity component w in Fig. 14.

The simulations have shown that on the truncated domain the newly proposed CPD condition is able to provide a solution that is closer, at least qualitatively, to the reference solution obtained on a much larger domain. The flow patterns and

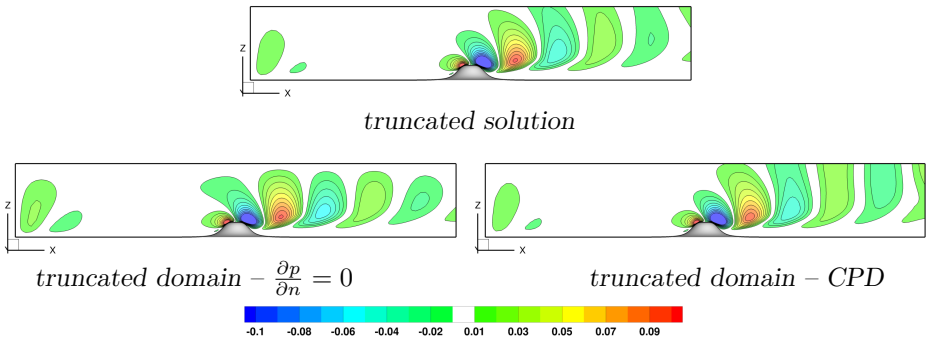

FIGURE 12. Contours of the vertical velocity component w - nondimensionalized $\widetilde{w} = w/U_*$.

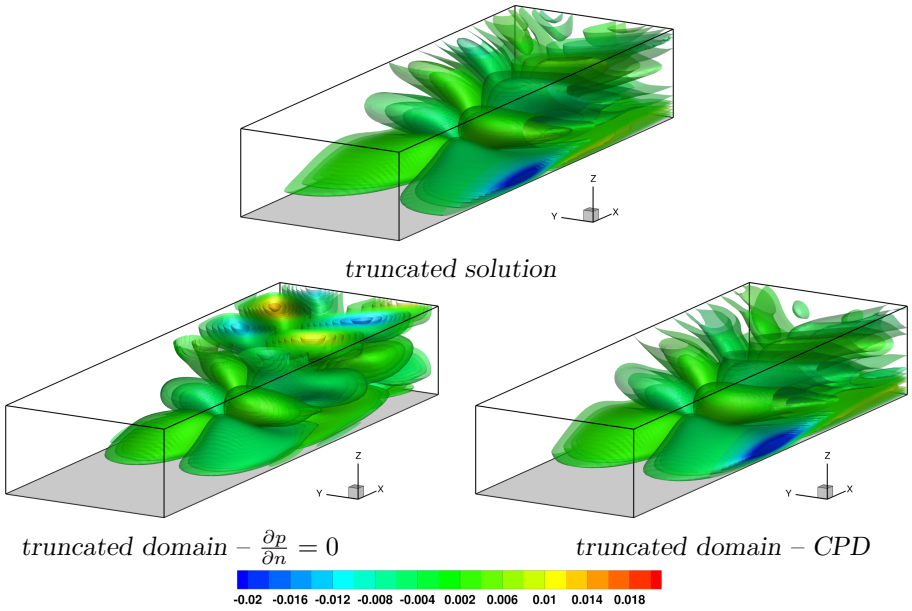

FIGURE 13. Isosurfaces of the transversal velocity component v - nondimensionalized $\widetilde{v} = v/U_*$.

characteristics are well preserved, despite the severe truncation of the computational domain. The ability to offer "flow-transparent" far-field boundary conditions, makes more likely to accept the truncated domain solution in the whole domain, up to the boundary, without the need of cut-off the evidently non-physical solution in the regions close to the far-field boundaries, like in the case of homogeneous Neumann pressure condition. This might, e.g., be of a crucial importance in evaluating certain physical fluxes across the boundaries, or in the case of models coupling on nested grids.

3.3. **Some additional results.** From the presented simulations and the comparison of the truncated domain solution with the reference solution obtained on the

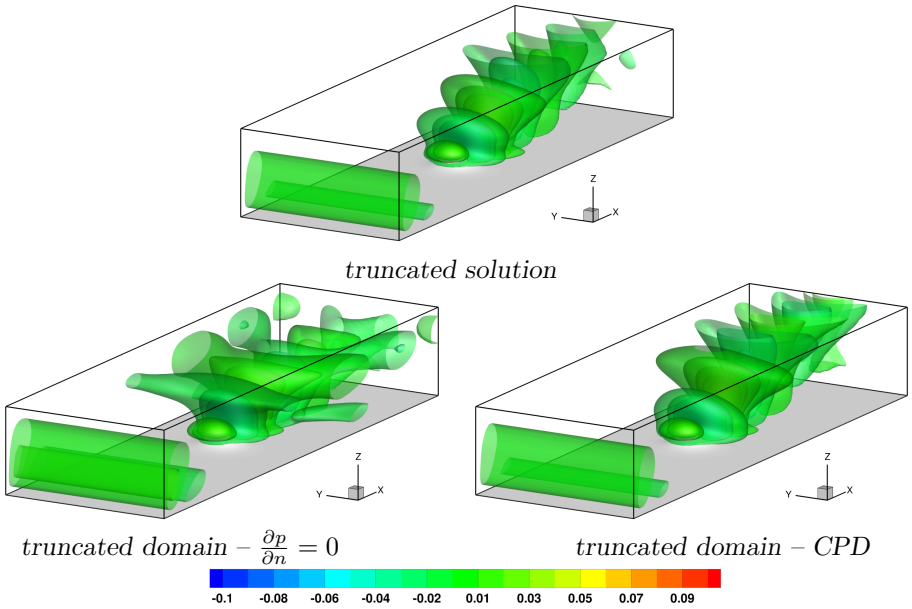

FIGURE 14. Isosurfaces of the vertical velocity component w - nondimensionalized $\widetilde{w} = w/U_*$.

larger domain a natural question arises whether the choice of the reference solution was right and how this choice affects the conclusions being made from the comparisons.

As mentioned earlier, the reference solution was obtained on a larger computational domain using the CPD condition in the far field. The larger domain was, compared to the standard truncated one, extended up (made thicker in the vertical z direction) and also extended laterally (made wider in the transversal y direction) on both sides. The size of the extension (boundary shift) was chosen $H = L_z/2 = (L_y/2)/2$. So the question can be posed, what if an even bigger domain will be used to get the reference solution, and what if the homogeneous Neumann pressure condition will be used on the far-field boundaries? In order to be able to give at least some qualitative answer, a series of additional simulations was performed. Besides the standard truncated domain and the already used domain extended by $+H$, a third domain was adopted where the upper and lateral boundaries are shifted further by another H, being now shifted by $+2H$ with respect to the original truncated domain. Simulations were run on all three domains, using both, the classical homogeneous Neumann and the new CPD pressure conditions in the far field.

Although the full 3D simulations were performed, only the 2D cuts in the plane of symmetry are shown. Besides of the already presented vertical velocity w contours, also the pressure p and longitudinal velocity u contours are shown for all six cases.

Starting with the pressure field shown in Fig. 15, the two initial observations can be made. First, in the left column, where the homogeneous Neumann condition was used, the isolines really enter the upper boundary vertically, being perpendicular to the boundary. So the solution really respects the imposed (enforced) pressure boundary condition. Second, when looking at the shape of the contours close to the

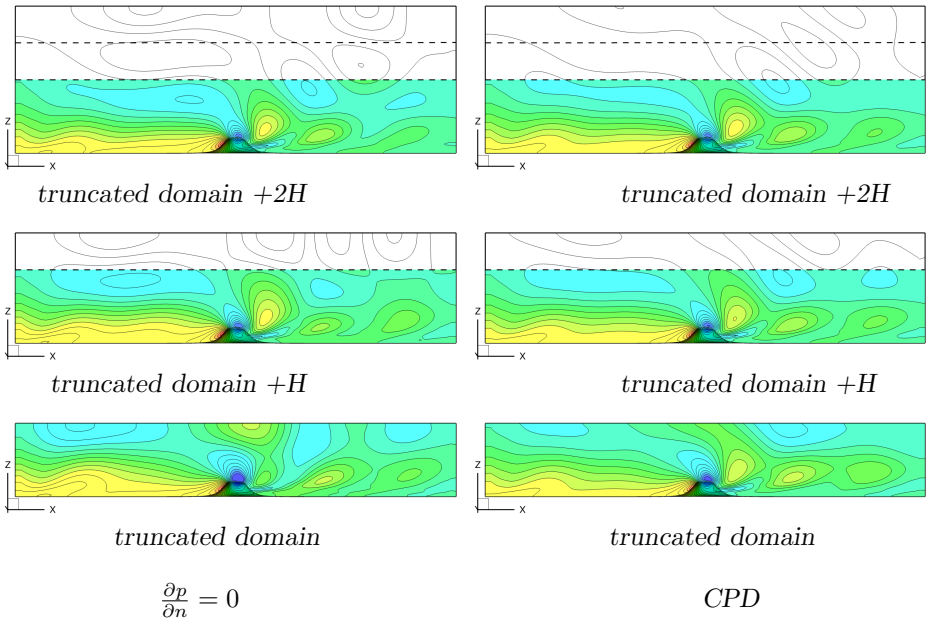

FIGURE 15. Pressure contours in the plane of symmetry.

assumed artificial boundaries of the smaller domains (marked by a dashed line), it is evident that the contours are far from being perpendicular to these "boundaries". So enforcing the homogeneous Neumann condition for pressure would certainly affect the solution. On the other hand, the use of the CPD condition gives much reasonable slopes of the contours close to the boundary. From the comparison of the pressure fields for the three domain sizes, it can be seen that the domain truncation has much smaller impact on the solution, when the CPD condition is used. A very similar conclusion can be drawn also from the longitudinal (Fig. 16) and especially vertical velocity contours (Fig. 17). The homogeneous Neumann condition leads to very different solutions for different domain sizes. The CPD condition however seems to reduce the effect of the domain size on the solution. Even for the smallest truncated domain, the solution obtained using the CPD condition is comparable with the one obtained on a much larger domain (preserving its main characteristic features).

The comparisons presented in Figs. 15–17, document and justify the choice of the middle sized ($+H$ extended) domain with the CPD condition for the relevant reference solution. Although this choice affects (to some extent) the comparisons being made between the truncated reference solution and the truncated domain solution, these differences do not change the conclusions being made from it.

4. **Conclusions & Remarks.** The convective pressure derivative boundary condition (6) performed very well in our numerical simulations. The obvious alteration of the solution close to boundaries was minimalized while retaining the numerical convergence for this simulation.

- *Physical interpretation/justification of the CPD condition* – The ad-hoc proposed formula (6) for pressure was based on our previous experience with

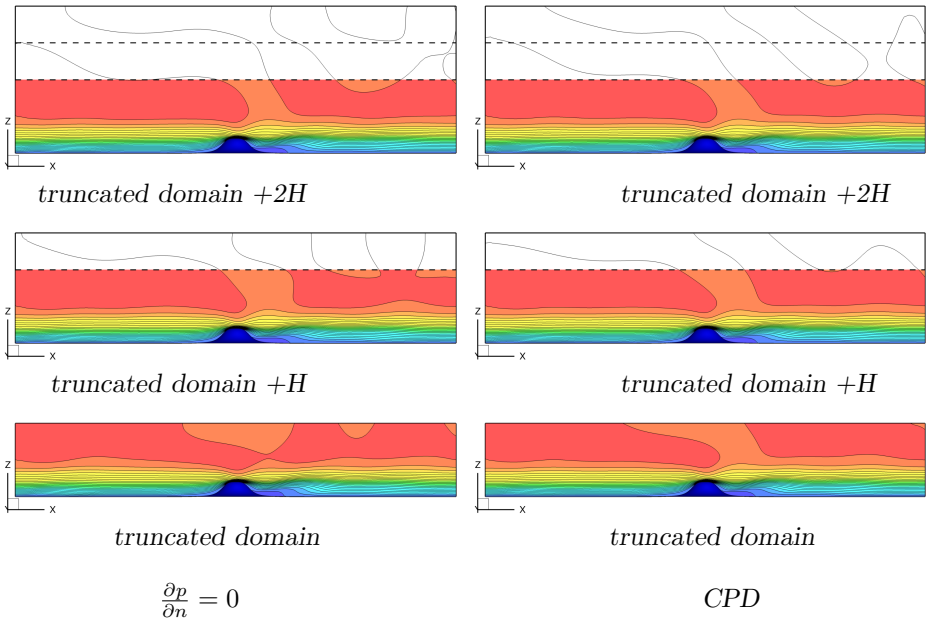

FIGURE 16. Longitudinal velocity contours in the plane of symmetry.

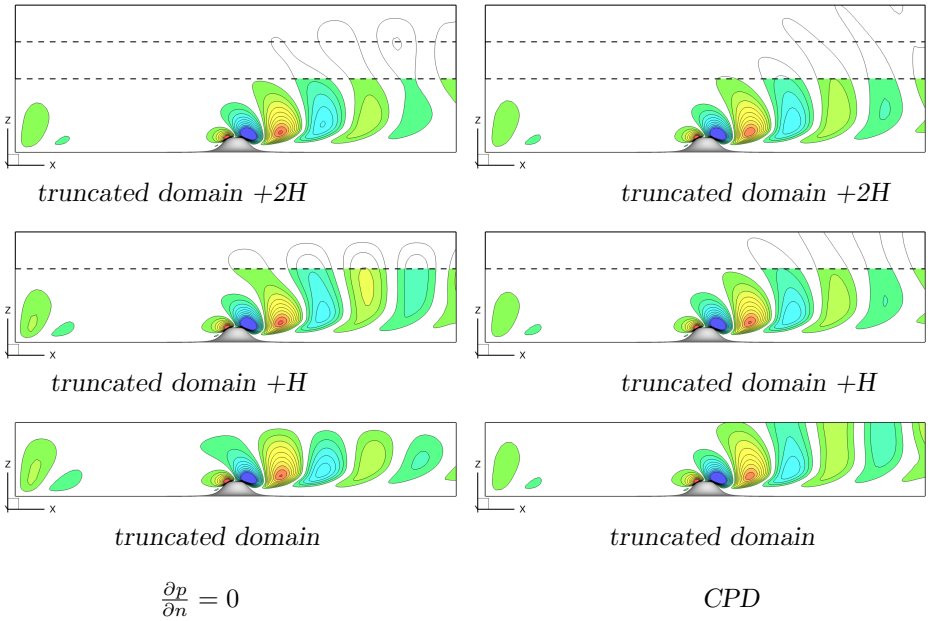

FIGURE 17. Vertical velocity contours in the plane of symmetry.

numerical solution of this type of flows. The importance of the term $\frac{\partial u_n}{\partial n}$ is really essential. It can be better understood when a local coordinate system is adopted at an artificial boundary point. Let us, e.g., assume that the (outer)

normal direction is associated with the z axis, while the x and y axes now define a tangential plane (to boundary). Due to incompressibility, i.e., due to the divergence-free constraint $u_x + v_y + w_z = 0$, the value of normal derivative of normal velocity component w_z indicates to what extent the tangential, two-dimensional continuity equation $u_x + v_y = 0$ is satisfied, i.e. $u_x + v_y = -w_z$. So, when $w_z = 0$, the flow field can be seen as locally two-dimensional and it makes a sense to drop the pressure derivative in the third (normal) direction. Any imbalance of this local two-dimensionality of the flow field leads to the appearance of the normal pressure derivative. In the absence (or negligibility) of local viscous forces, the pressure gradient should compensate the inertia represented by the convective term. Thus the proportionality factor (with respect the normal velocity normal derivative $\frac{\partial u_n}{\partial n} = w_z$) was set to $\rho^*|\boldsymbol{u}|$, which assures the proper (convective term like) scaling and is invariant to the orientation of the chosen coordinate system. In the case solved in this paper the velocity $\boldsymbol{u}$ at the far-field was almost parallel to the boundary, so $|\boldsymbol{u}_\tau| \approx |\boldsymbol{u}|$, so there is still an open question whether e.g. use of $|\boldsymbol{u}_\tau|$ instead of $|\boldsymbol{u}|$ would not give better results in some other configurations.

- *No-slip wall & Inlet* – It is good to note that at the no-slip wall (where $|\boldsymbol{u}| = 0$) the CPD condition (6) reduces to the classical homogeneous Neumann pressure condition. Also at the inlet, where $\frac{\partial u_n}{\partial n}$ vanishes (e.g., due to prescribed $u_\tau = 0$) the homogeneous Neumann condition for pressure is recovered. So, in fact, we can claim, that in our case we have used the CPD condition on all boundaries, except the outlet.
- *Outlet pressure condition* - In this (variable density, stratified) case the outlet pressure was simply set to a constant. This choice is obviously not optimal but has only minor influence on the upstream flow field. The variable density case behaves much more like a compressible flow where the pressure should be prescribed (by a Dirichlet condition) on the subsonic outlet. On the other hand, the homogeneous (constant density, non-stratified) case was successfully tested as well, with the CPD condition (6) used on all boundaries.
- *Velocity at the far-field boundaries* – The (linear) extrapolation[6] of all velocity components used in this study seems to work well for the solved test case. The possibility of using the homogeneous Neumann condition for the tangential components of velocity[7] (while keeping the extrapolation for the normal one), was successfully tested. It has only marginal (but yet visible) effect on the solution close to the boundary. Its use however can be of some importance in the theoretical analysis of the model.
- *Other numerical methods* – The results presented in this paper were obtained using a finite-difference discretization on a structured grid. Pressure was computed using the artificial compressibility method. The finite-volume simulations on the same grid, using also the artificial compressibility method, gave identical results for the solved cases. The question is, what could be the effect of unstructured grids and e.g. pressure correction methods on the efficiency of the proposed CPD condition. Technically, the implementation should be straightforward, as the CPD condition (6) is nothing but a non-homogeneous

[6]The linear extrapolation is equivalent to the use of one-sided (backward) first order approximation of derivatives at the boundary points.

[7]Motivated by the same approach as used in the do-nothing condition (5).

Neumann condition applied to pressure. The implementation in the finite element case is also still an open question.

In summary, the presented setup, using the prescribed profile of velocity and density at the inlet, given pressure at the outlet and no-slip condition for the velocity at the wall, combined with velocity extrapolation and CPD pressure condition (6) in the far-field proved to work well (best from all the setups we have tested so far) in the numerical simulations for this specific case. It is usable both in the variable density (stratified) case as well as in the homogeneous, constant density case.

The theoretical study of the well-posedness of the problem using this boundary setup should be provided in order to better understand and justify its use. In addition further numerical simulations have to be performed to verify the suitability of this artificial boundary conditions setup for other geometrical and physical configurations.

Acknowledgments. The financial support for the present work was provided by the Czech Science Foundation under the grants No. 16-03230S and 19-04243S. Tomáš Bodnár is grateful for the invited professorship position he received at the University of Toulon, which has made possible this joint work. The authors acknowledge the co-funding from the Erasmus+ Programme of the European Union.

REFERENCES

[1] T. Bodnár and L. Beneš, On some high resolution schemes for stably stratified fluid flows, in *Finite Volumes for Complex Applications VI, Problems & Perspectives*, vol. 4 of Springer Proceedings in Mathematics, Springer Verlag, 2011, 145–153.

[2] T. Bodnár, L. Beneš, P. Fraunié and K. Kozel, Application of compact finite-difference schemes to simulations of stably stratified fluid flows, *Applied Mathematics and Computation*, **219** (2012), 3336–3353.

[3] T. Bodnár and P. Fraunié, On the boundary conditions in the numerical simulation of stably stratified fluids flows, in *Topical Problems of Fluid Mechanics 2017*, Institute of Thermomechanics CAS, Prague, 2017, 45–52.

[4] T. Bodnár and P. Fraunié, Artificial far-field pressure boundary conditions for wall-bounded stratified flows, in *Topical Problems of Fluid Mechanics 2018*, Institute of Thermomechanics CAS, Prague, 2018, 7–14.

[5] T. Bodnár, P. Fraunié and H. Řezníček, Numerical tests of far-field boundary conditions for stably stratified stratified flows, in *Topical Problems of Fluid Mechanics 2019*, Institute of Thermomechanics CAS, Prague, 2019, 1–8.

[6] M. Braack and P. Mucha, Directional do-nothing condition for the Navier-Stokes equations, *Journal of Computational Mathematics*, **32** (2014), 507–521.

[7] L. Ding, R. J. Calhoun and R. L. Street, Numerical simulation of strongly stratified flow over a three-dimensional hill, *Boundary-Layer Meteorology*, **107** (2003), 81–114.

[8] J. Heywood, R. Rannacher and S. Turek, Artificial boundaries and flux and pressure conditions for the incompressible Navier-Stokes equations, *International Journal for Numerical Methods in Fluids*, **22** (1996), 325–352.

[9] J. C. R. Hunt and W. H. Snyder, Experiments on stably and neutrally stratified flow over a model three-dimensional hill, *Journal of Fluid Mechanics*, **96** (1980), 671–704.

[10] P. Marchesiello, J. McWilliams and A. Shchepetkin, Open boundary conditions for long-term integration of regional oceanic models, *Ocean Modelling*, **3** (2001), 1–20.

[11] I. Orlanski, A simple boundary condition for unbounded hyperbolic flows, *Journal of Computational Physics*, **21** (1976), 251–269.

Received xxxx 20xx; revised xxxx 20xx.

E-mail address: Tomas.Bodnar@fs.cvut.cz
E-mail address: Philippe.Fraunie@univ-tln.fr
E-mail address: knobloch@karlin.mff.cuni.cz
E-mail address: Hynek.Reznicek@fs.cvut.cz